Ghost red blood cells for enhanced particle detection with defocusing PTV in microcirculation experiments

Gonçalo Coutinho[1,*], Philipp Warlitz[3], A. Rita Silva-Santos[4], Ricardo M. Silva[4], Ana Moita[1], Duarte Miguel F. Prazeres[4], Jochen Kriegseis[3], António L. N. Moreira[1], Massimiliano Rossi[2]

1: IN+ Center for Innovation, Technology and Policy Research, Instituto Superior Técnico, University of Lisbon, Portugal
2: Department of Industrial Engineering, Alma Mater Studiorum, University of Bologna, Italy
3: ISTM Institute of Fluid Mechanics, Karlsruhe Institute of Technology, Germany
4: iBB Institute for Bioengineering and Biosciences, Instituto Superior Técnico, University of Lisbon, Portugal
*Corresponding author: goncalo.coutinho@tecnico.ulisboa.pt

Keywords: 3D Particle tracking velocimetry, General defocusing particle tracking, Red blood cells, Ghost red blood cells, Platelet-size particles, 3D Flow characterization.

ABSTRACT

Particle tracking of rigid fluorescent particles in microcirculation environments is often found to be difficult, since the presence of red blood cells (RBCs) at physiologically relevant conditions (i.e., hematocrit (Hct) of $30-40\,\%$) masks the particle images. In turn, making particle detection challenging. To overcome this difficulty, we propose to use ghost RBCs for enhanced particle detection. These are quasi-transparent RBCs obtained by removing the hemoglobin from normal RBCs. To understand whether the ghost RBCs can improve the particle detection, we performed defocusing particle tracking measurements with the general defocusing particle tracking (GDPT) method of the rigid fluorescent particles in normal and ghost RBC flows. The measurements were performed at Hct of $30\,\%$ and for three different flow rates: $Q = [0.14,\, 0.48,\, 0.64]\,\mu$L/min. From the three-dimensional particle trajectories, we evaluated the correlation coefficient from the GDPT evaluations and compared the fluid dynamic behaviour of the two types of cells. Overall, the results show that ghost RBCs are an attractive solution for this type of experiments, since they improve the correlation coefficients up to values similar to cell-free experiments, while exhibiting a fluid dynamic behavior similar to normal RBCs i.e., in terms of velocity and relative viscosity data.

1. Introduction

Microcirculation studies focused on the behavior of rigid particles in red blood cell (RBC) flows are mostly limited to simulation-driven research. This is primarily attributed to the complexity of the flow, which for in-vitro experiments has challenging measurement conditions. To begin with, the particle behavior exhibits a three-dimensional (3D) nature (Vahidkhah et al., 2014; Závodszky et al., 2019). In other words, besides longitudinal, they also exhibit lateral and vertical displacements. Additionally, the presence of the RBCs at physiologically relevant concentrations (Hct=$30-40\,\%$)

masks the particle images of the rigid particles, making particle detection in in-vitro experiments challenging (Carboni et al., 2016).

When it comes to experiments, particle-based velocimetry methods are non-intrusive, optical measurement techniques, well-known for providing quantitative measurements of the two-dimensional velocity. These include classical approaches such as micro particle image velocimetry (µPIV) and micro particle tracking velocimetry (µPTV) see e.g., Lindken et al. (2009). However, due to the 3D nature of the particle dynamics, µPIV and µPTV methods are an oversimplification of the problem. To capture the 3D nature of the particle dynamics, Coutinho et al. (2023) recently proposed the use of a defocusing particle tracking (DPT) method referred to as general defocusing particle tracking (GDPT) (Barnkob & Rossi, 2020; Rossi & Barnkob, 2020). Although the authors were able to track the particles in RBC flows in all three dimensions (x, y, z), they still experienced some difficulties in particle detection. As similarly reported in the µPTV measurements of Carboni et al. (2016), the RBCs were found to mask the particle images, therefore degrading the correlation coefficient in GDPT evaluations. Such masking effects were additionally responsible for the increased uncertainty in the out-of-plane component.

A possible solution for the RBC-induced masking is the use of ghost RBCs i.e., hemoglobin-free RBCs. Briefly, the RBCs undergo a process where the hemoglobin is removed from the cells, resulting in quasi-transparent cells with similar shape and size to normal RBCs. Such treatment makes them an attractive solution to improve DPT measurements in microcirculation experiments. Accordingly, the present work aims to compare the use of normal and ghost RBCs in microcirculation experiments with rigid particles. Our primary goal is to understand whether the use of ghost RBCs can improve the correlation coefficient in GDPT evaluations, while additionally comparing the fluid dynamic behavior of both cell types i.e., normal and ghost RBCs, in terms of velocity profiles and relative viscosity.

2. Materials and methods

2.1. Preparation of normal and ghost red blood cells samples

The RBCs suspensions were prepared from bovine washed RBCs (IBORBC100P, Innovative Research Co., USA). To obtain a hematocrit level of Hct=$30\,\%$, the initial RBC solution was diluted in phosphate-buffered saline (PBS) ($\times 1.0$, ph=7.4, FisherScientific Co., USA) (Carboni et al., 2016; Coutinho, Moita, Rossi, & Moreira, 2023). Preparation of RBC ghosts was performed based on the procedure reported byJamiolkowski et al. (2015). Briefly, 4 mL of $30\,\%$ RBCs suspension was mixed with 36 mL of a lysing solution containing 4 mM $MgSO_4$, 25 mL/L of PBS, and acetic acid until pH 5.2. The solution was left to rest overnight at 4ºC, after which the pH was brought back to the physiological norms of 7.8. Ultimately, the solution was incubated at 37 ºC for 1 hour to promote cell reseal. The solution was then centrifuged at 15,000 g for 30 minutes and the supernatant was discarded. Ghost RBCs were washed 2 times with PBS buffer through centrifugation under the

same aforementioned conditions. On the last washing step, the volume of ghost cells was determined and the volume of PBS was adjusted to a final Hct=30 % in PBS with 100 mg/L gentamicin (NZYTech, Lisbon, Portugal). A comparison between the normal and ghost RBCs is already given in Fig. 1(c), where we show bright-field, color-coded images of the two types of cells flowing inside a microchannel. Ultimately, rigid fluorescent spherical particles (530/607 nm, PS-FluoRed, MicroParticles GmbH, Germany) with nominal diameter of 2.47 µm were added to the solutions of normal and ghost RBCs samples.

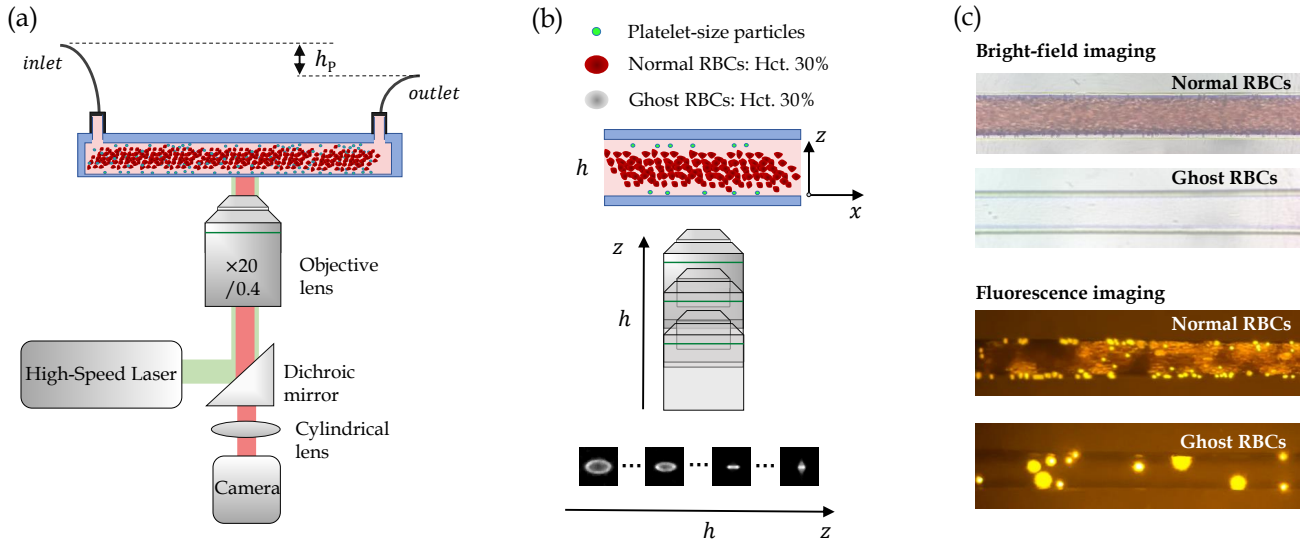

Figure 1. (a) Schematic of the experimental setup used to perform the GDPT measurements. (b) Schematic of the acquisition of the calibration image stack.(c) Sample color-code images of flow with normal and ghost RBCs, using bright-field and fluorescence imaging without the cylindrical lens.

2.2. Experimental setup

The general schematic of the experimental setup is provided in Fig. 1(a). The microchannel was placed on the working stage of an epi-fluorescent inverted microscope (DM IL LED, Leica Microsystems GmbH, Germany) equipped with a high-speed camera (HighSpeedStar 4G, LaVision GmbH, Germany). The system was operated with a $\times 20/0.4$ objective lens (NPlan Epi, Leica Microsystems GmbH, Germany), together with a cylindrical lens ($f_{\text{cyl}} = 500$ mm) (LJ1144RM-A, Thorlabs Inc., USA) placed at a distance of 60 mm in front of the camera sensor. This yielded a spatial resolution of $0.76\,\mu$m and $0.67\,\mu$m in the x- and y-direction, respectively. The present configuration used a backlight illumination provided by a high-speed laser (527 nm Nd: YLF LDY 300, Litron Lasers, UK) operated at 45%, and in synchronization with the high-speed camera through LaVision software DaVis 8. The system also included a filter cube for fluorescence imaging (Excitation: BP 525/50 nm; Dichroic: 570nm and Emission: 620/60 nm). The measurements were

performed in a microchannel with a square cross-sectional area of $w_{\mathrm{ch}} \times h_{\mathrm{ch}} = 50 \times 50\,\mu\mathrm{m}^2$ and length of $l_{\mathrm{ch}} = 58.5\,\mathrm{mm}$ (CS-10000087, Darwin Microfluidics, France). The microchannel is made of a rigid polymer (Topas COC), see Fig. 1(a). In all measurements, the pressure-driven flow was imposed by hydrostatic pressure, which was obtained by an offset (h_{p}) between the inlet and collection reservoir. The selected flow rates were determined by measuring the Poiseuille flow of a PBS solution i.e., in the absence of RBCs: $Q = [0.14,\ 0.48,\ 0.64]\,\mu\mathrm{L/min}$, yielding wall-shear rates of $\dot{\gamma} = [134.49,\ 453.47,\ 609.21]\,\mathrm{s}^{-1}$, see Son (2007). To ensure the reproducibility of the results, the measurements were repeated three times per flow rate for the normal and ghost RBCs samples. Between measurements, the whole system was flushed and the microchannel rinsed with distilled water. Additionally, the RBC suspensions were gently agitated before each measurement to avoid sedimentation.

2.3. General defocusing particle tracking

To determine the 3D coordinates (x, y, z) and velocity components (v_x, v_y, v_z) of the tracer particles in the normal and ghost RBC-suspension flows, we use a single-camera 3D PTV method known as GDPT (Barnkob & Rossi, 2020; Rossi & Barnkob, 2020). Here, x and y represent the in-plane coordinates, with x defined along the main flow direction as depicted in Fig. 1(b); z is the out-of-plane component, defined along the depth of the channel, see Fig. 1(b). For optical setups providing particle images that vary solely with depth coordinate, the method takes advantage from the depth-dependent shape of particle images to determine the depth position. The spherical tracer particles used in our experiments exhibit unique defocused particle images depending on their position along the optical axis i.e., their depth position, see Fig. 1(b). As such, the 3D positions of the particles are recovered using a suitable mapping of the defocused particle images for the depth coordinate (z), and the in-plane coordinates (x, y) are obtained from the center of the particle images. The mapping consists of a calibration image stack, which is obtained by taking images of a tracer particle sedimented on the bottom of the microchannel and adjusting the depth position by moving the objective lens (Fig. 1(b)). In our measurements, the calibration stack was obtained by adjusting the focus position of the objective lens at constant steps of 1 micron.

The measurements were performed near the center of the channel ($\Delta x = 29\,\mathrm{mm}$; $\Delta x / l_{\mathrm{ch}} \approx 50\,\%$). The flow was recorded using a total of 6000 dark-field images of the fluorescent spherical particles, where the frame rate was varied between $350\,\mathrm{Hz}$ and $750\,\mathrm{Hz}$ depending on the working fluid and flow rate. The images were processed using DefocusTracker (Barnkob & Rossi, 2021). The particle detection was performed by matching the experimental to the calibration defocused particle images through normalized cross-correlation (Lewis, 1994). For each defocused particle image, the correlation coefficient C_m translates the goodness of the particle image matching and takes values between 0 and 1, with 1 corresponding to a perfect match (Rossi & Barnkob 2020). We will continue the discussion later in Sec. 3.1. As for the tracking, we used the nearest-neighbor algorithm (Malik et al., 1993), since the particle density was low. The reader can have access to DefocusTracker through the following link: `https://gitlab.com/defocustracking`.

In DPT experiments in microfluidic environments, the measured particle coordinates are typically biased due to the presence of the field curvature aberration and refraction (Cierpka et al., 2010; Rossi et al., 2012). Regarding the former, the particle coordinates were corrected using a procedure based on a reference measurement of a Poiseuille flow i.e., using the PBS measurements, as described in Coutinho et al. (2023). Refraction was corrected using the refractive index of the fluid, which is approximately $n_f = 1.33$.

3. Results

3.1. Correlation coefficient in GDPT measurements

To evaluate the impact of normal and ghost RBCs in particle detection, Fig. 2 shows the correlation coefficient C_m as a function of the out-of-plane coordinate z obtained from the GDPT evaluations for the considered flow rates Q. The results are shown for a single measurement and include the median value of C_m and 80 % distribution of the dataset. Besides, the threshold of $C_m = 0.85$ was set based on our previous work, see Coutinho et al. (2023). Please note that as introduced in Sec. 2.3, C_m varies between 0 and 1, where 1 corresponds to a perfect match of the defocused particle image.

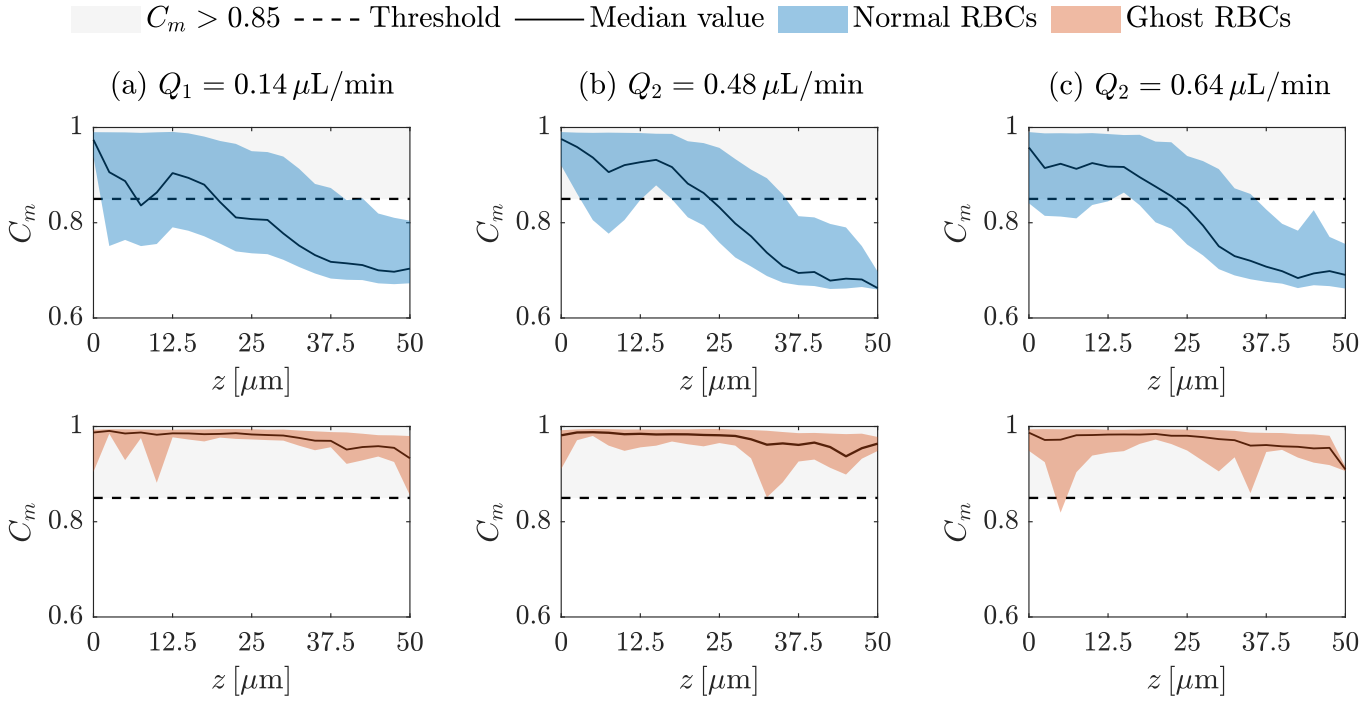

Figure 2. Distribution of the correlation coefficient C_m as a function of z obtained from the GDPT evaluations for normal and ghost RBCs at different flow rates. (a) $Q_1 = 0.14\,\mu$L/min. (b) $Q_1 = 0.48\,\mu$L/min. (c) $Q_1 = 0.64\,\mu$L/min

As recently observed by Coutinho et al. (2023), in the presence of normal RBCs the data shows a large dispersion and we can observe a degradation of C_m as z increases (first row in Fig. 2). This comes with no surprise as we move deeper into the flow i.e., larger z, more RBCs are flowing between the fluorescent particles and our objective lens. As a consequence, there is a larger RBC-induced masking of the defocused particle images. Such an effect is also the cause for the larger uncertainty in the out-of-plane component z in this type of experiment. On the other hand, the results with ghost RBCs show correlation coefficients C_m similar to those found in cell-free experiments. First, the median value of C_m sits above the threshold ($C_m > 0.85$). Second, we observe a smaller dispersion of the data points. Overall, the results from Fig. 2 show that in what concerns DPT, ghost RBCs can improve the particle detection. Yet, it remains to be clarified if the fluid dynamic behavior of both types of cells is similar. In the following Sec. 3.2, we compare the velocity profiles and relative viscosity of normal and ghost RBCs.

3.2. Flow characterization

Up to this point, we have shown that by using ghost RBCs in microcirculation experiments one can improve the correlation coefficient in the GDPT evaluations, hence improving particle detection. It remains now to be clarified whether the fluid dynamic behavior is similar to that of normal RBCs. To that end, we compare the velocity data $v_x(y, z)$ of the fluorescent particles in normal and ghost RBCs flows at different flow rates. For visualization, the velocity data was projected along the y and z directions and fitted to an empirical equation derived from the solution of the Poiseuille flow in straight-square channels

$$v_x = v \cdot \left(\frac{\cosh(0.5^m) - \cosh(|y^*|^m)}{\cosh(0.5^m) - 1} \right) + v_0, \tag{1}$$

where v and v_0 are the fitting parameters based on the velocity distribution (v_x), and m is a fitting parameter based on the velocity profile bluntness see, e.g., Passos et al. 2019. The coordinate y^* is normalized with the width w_{ch} of the microchannel. The same expression is valid for the vertical direction z, with the coordinate being normalized with the height h_{ch} of the microchannel. For the normal RBCs, we have additionally assumed symmetry in the z-direction, and the measured data was mirrored with respect to the center of the channel to compensate for missing information along the depth of the channel. The results are shown in Fig. 3. For comparison, we also plot the velocity data of the base flow, i.e. the PBS solution.

The difference between the base flow (i.e., PBS solution), and normal and ghost RBCs is remarkable. Whereas for the PBS measurements, the velocity information resembles the classical Poiseuille flow (Bruus, 2008), for the normal and ghost RBCs we can observe a blunter velocity profile, typical of RBCs flows in capillary-size microchannels (Carboni et al., 2016). Regarding the two types of cells, the results shown in Fig. 3 highlight the resemblance of the fluid dynamic behavior of the ghost RBCs when compared to that of normal RBCs. First in terms of the shape of the velocity

profiles, and second in terms of the velocity magnitude. Besides, as already shown in Sec. 3.1, by using the ghosts we improve the particle detection in the GDPT measurements. Accordingly, there is a smaller scatter of the velocity data, while additionally providing the velocity data across the entire depth of the channel i.e., without the need to mirror the data (e.g., Fig. 3(b)).

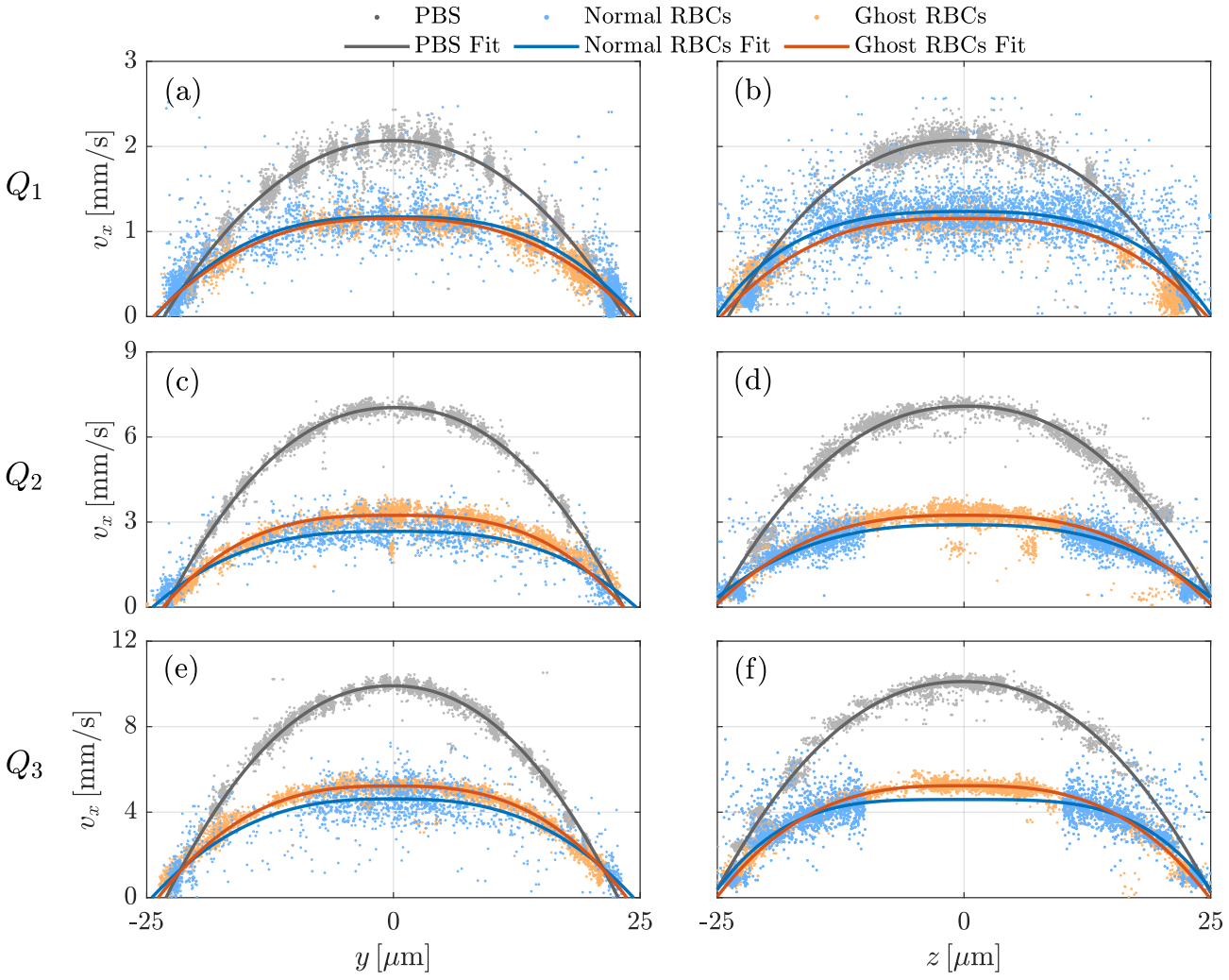

Figure 3. Scatter and fitted velocity profiles v_x based on Eq. (1), including the PBS, normal RBCs, and ghost RBCs measurements for the three flow rates, Q1, Q2, and Q3. (a), (c) and (e) v_x along the y direction. (b), (d) and (f) v_x along the z direction.

To further compare the fluid dynamic behavior of the two types of cells, the maximum velocity of each profile was calculated using the fitted curves from Fig. 3 and it is shown in Fig. 4(a). The results represent the mean value of the consecutive measurements and the error bars show the root mean square of error (rmse) from the fitting function. Again, the present results highlight the similar fluid dynamic behavior between normal and ghost RBCs, and the distinct behavior

when compared to a Poiseuille flow. The larger error bars for the normal RBCs are most likely a consequence of the RBC-induced masking: A coarser correlation coefficient (C_m) is accordingly expected to increase the measurement uncertainty.

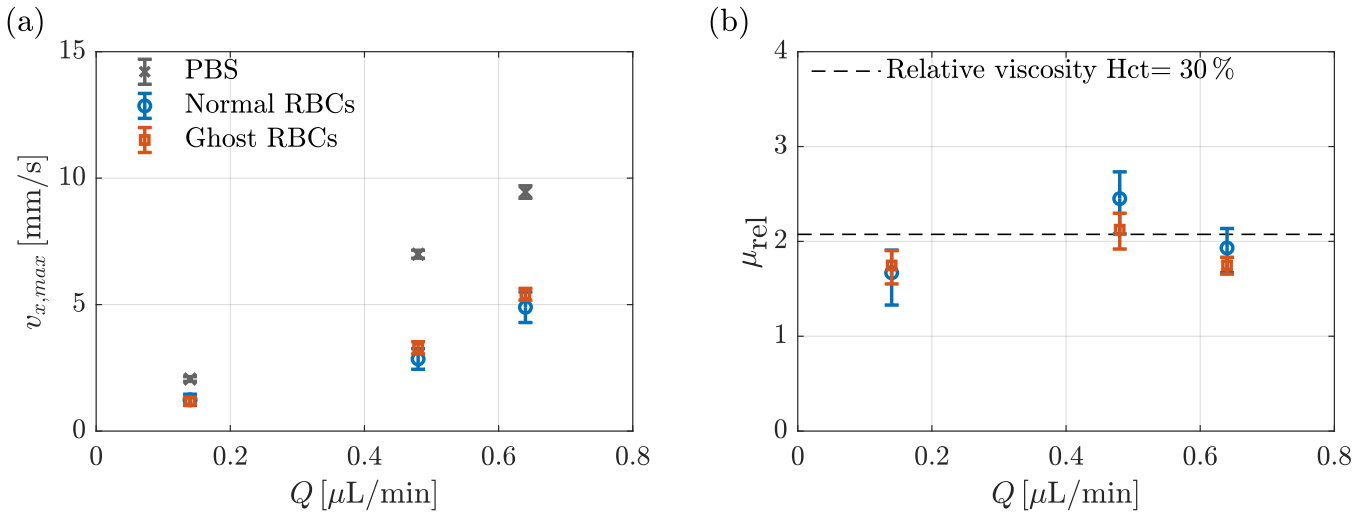

Figure 4. (a) Maximum velocity $v_{x,max}$ for the PBS, normal and ghost RBCs measurements, including the three flow rates. (b) Relative viscosity of normal and ghost RBCs, for the three flow rates. The reference line represents the expected relative viscosity based on the empirical model from Pries et al. 1992, for RBC flows in a capillary sized channel ($D_{\mathrm{ch}} = 55$µm) at Hct=30%. Error bars are included based on the root mean square of the error from the velocity fitting function.

Another relevant property of RBC flows is viscosity. It is well-known that the viscosity of RBC solutions increases with hematocrit (Hct) (Pries et al., 1992), hence being also a measure of similar fluid dynamic behavior between normal and ghost RBCs. Since RBC flows have a non-Newtonian behavior in micro-sized channels, the viscosity is here calculated as a relative viscosity. Following the work of Pries et al. (1992), the expression for the relative viscosity yields the ratio between flow rates, PBS and RBCs, according to Eq. (2). More details are also given in Coutinho et al. (2023).

$$\mu_{\mathrm{rel}} = \frac{Q_{\mathrm{PBS}}}{Q_{\mathrm{RBC}}}, \tag{2}$$

where Q_{RBC} and Q_{PBS} represent the flow rate with and without flowing RBCs, respectively. The same expression is valid for the ghost RBCs. For comparison with previous studies, we compare the measured values of the relative viscosity with the empirical model given by Pries et al. (1992).

$$\mu_{rel} = 1 + B[(1 - \mathrm{Hct})^C - 1]. \tag{3}$$

The fitting parameters B and C were obtained from the measurements of Bayliss (1952) in a microchannel with a tube diameter of $D_{\mathrm{ch}} = 55$ µm. These values were selected based on the available

data and since the conditions were similar to the current experiments. The results of the relative viscosity μ_{rel} including all three flow rates are shown in Fig. 4(b), and represent a mean value. The added error bars are based on the rmse from the velocity fitting function (Eq. (1)).

The results from Fig. 4(b) again show the resemblance between normal and ghost RBCs, where the differences found between the two types of cells are within the rmse of the velocity fitting function. In addition, the measured values show a good correlation with the empirical model, as shown by the dashed line. As already discussed, the present results highlight the resemblance of the fluid dynamic behavior between normal and ghost RBCs, thus making the latter an attractive solution for DPT measurements in microcirculation experiments.

4. Conclusions

The present work shows that ghost RBCs can be used for enhanced particle detection with DPT in microcirculation experiments. The analysis of the correlation coefficients from the GDPT evaluations shows that ghost RBCs overcome the difficulties in detecting rigid, fluorescent particles in the presence of normal RBCs at physiological relevant concentrations (Hct=$30-40\,\%$). Regarding the fluid dynamic behavior, the velocity and relative viscosity data demonstrate the resemblance between normal and ghost RBCs. Overall, the present results make ghost RBCs an attractive solution for this type of experiment: improving the quality of the measurements and mimicking the fluid dynamic behavior of normal RBCs. Future work will address the dynamics of the rigid particles in normal and ghost RBC flows: particle diffusivity and drift velocity. Since the ghost RBCs lack the hemoglobin, it remains the question on whether the particle dynamics is similar to that observed in normal RBC flows.

Acknowledgements

Gonçalo Coutinho (GC) acknowledges the PhD scholarship 2021.04780.BD attributed by Fundação para a Ciência e Tecnologia (FCT). Massimiliano Rossi acknowledges the financial support by the VILLUM foundation under the Grant No. 00036098. Gonçalo Coutinho, Ana Moita, and António Moreira acknowledge Fundação para a Ciência e a Tecnologia (FCT) for partially financing the research through Project Ref. PTDC/EME-TED/7801/2020 and to funding through 2022.03151.PTD and LA/P/0083/2020 IN + -IST-ID and through UIPD/50009/2020-FCT and UIDB/50009 – FCT. A. Rita Silva-Santos, Ricardo M. Silva, and Duarte Miguel F. Prazeres acknowledge FCT for the projects UIDB/0465/2020 and UIDP/04565/2020 of the Research Unit Institute for Bioengineering and Biosciences - iBB, and LA/P/0140/2020 of the Associate Laboratory Institute for Health and Bioeconomy - i4HB.

References

Barnkob, R., & Rossi, M. (2020). General defocusing particle tracking: fundamentals and uncertainty assessment. *Experiments in Fluids*, *61*(4), 110.

Barnkob, R., & Rossi, M. (2021). Defocustracker: A modular toolbox for defocusing-based, single-camera, 3d particle tracking. *Journal of Open Research Software*, *9*(1), 22.

Bayliss, L. (1952, 01). Rheology of blood and lymph. *Deformation and Flow in Biological Systems*, 355-418.

Bruus, H. (2008). *Theoretical microfluidics*. Oxford University Press.

Carboni, E., Bognet, B., Bouchillon, G. M., Kadilak, A., Shor, L., Ward, M. D., & Ma, A. (2016). Direct tracking of particles and quantification of margination in blood flow. *Biophysical Journal*, *111*, 1487–1495.

Cierpka, C., Rossi, M., Segura, R., & Kähler, C. J. (2010). On the calibration of astigmatism particle tracking velocimetry for microflows. *Measurement Science and Technology*, *22*(1), 015401.

Coutinho, G., Moita, A., Ribeiro, A., Rossi, M., & Moreira, A. L. N. (2023, 05). On the characterization of bias errors in defocusing-based 3d particle tracking velocimetry for microfluidics. *Experiments in Fluids*, *64*. doi:

Coutinho, G., Moita, A. S., Rossi, M., & Moreira, A. L. N. (2023, Oct). Experimental perspective on the mechanisms for near-wall accumulation of platelet-size particles in pressure-driven red blood cell suspension flows. *Phys. Rev. Fluids*, *8*, 103101. Retrieved from `https://link.aps.org/doi/10.1103/PhysRevFluids.8.103101` doi:

Jamiolkowski, M., Woolley, J., Kameneva, M., Antaki, J., & Wagner, W. (2015, 04). Real time visualization and characterization of platelet deposition under flow onto clinically-relevant opaque surfaces. *Journal of Biomedical Materials Research Part A*, *103*. doi:

Lewis, J. (1994). Fast template matching. *Vision Interface*, *95*.

Lindken, R., Rossi, M., Große, S., & Westerweel, J. (2009, 10). Micro-particle image velocimetry (piv): Recent developments, applications, and guidelines. *Lab on a chip*, *9*, 2551-67. doi:

Malik, N., Dracos, T., & Papantoniou, D. (1993). Particle tracking velocimetry in three-dimensional flows - part ii: Particle tracking. *Experiments in Fluids*, *15*, 279-294.

Passos, A., Sherwood, J., Kaliviotis, E., Agrawal, R., Pavesio, C., & Balabani, S. (2019, 09). The effect of deformability on the microscale flow behavior of red blood cell suspensions. *Physics of Fluids*, *31*, 091903.

Pries, A. R., Neuhaus, D., & Gaehtgens, P. (1992). Blood viscosity in tube flow: dependence on diameter and hematocrit. *American Journal of Physiology-Heart and Circulatory Physiology*, *263*(6), H1770–H1778. doi:

Rossi, M., & Barnkob, R. (2020). A fast and robust algorithm for general defocusing particle tracking. *Measurement Science and Technology*, *32*(1), 014001.

Rossi, M., Segura, C., R.and Cierpka, & Kähler, C. (2012). On the effect of particle image intensity and image preprocessing on the depth of correlation in micro-PIV. *Exp Fluids*, *52*, 1063–1075. doi:

Son, Y. (2007, 01). Determination of shear viscosity and shear rate from pressure drop and flow rate relationship in a rectangular channel. *Polymer*, *48*, 632-637. doi:

Vahidkhah, K., Diamond, S. L., & Bagchi, P. (2014). Platelet dynamics in three-dimensional simulation of whole blood. *Biophysical Journal*, *106*(11), 2529–2540.

Závodszky, G., van Rooij, B., Czaja, B., Azizi, V., Kanter, D., & Hoekstra, A. (2019, 03). Red blood cell and platelet diffusivity and margination in the presence of cross-stream gradients in blood flows. *Physics of Fluids*, *31*.